

RADIO RECOMBINATION LINE OBSERVATIONS OF THE C II REGION NGC 2023

G. R. KNAPP

Owens Valley Radio Observatory, California Institute of Technology

ROBERT L. BROWN

National Radio Astronomy Observatory*

AND

T. B. H. KUIPER

Jet Propulsion Laboratory, California Institute of Technology

Received 1974 July 22

ABSTRACT

The reflection nebula NGC 2023 has been observed at four frequencies in a study of its carbon recombination line emission. The observations show the recombination line region to be about 2 pc in diameter, with an average electron density of $\sim 0.2 \text{ cm}^{-3}$ and electron temperature of $\sim 20^\circ \text{ K}$. The electron density increases exponentially near the B1.5 star HD 37903, the illuminating star of NGC 2023. The most reasonable interpretation of the observational results is that the carbon emission lines arise in a cold C II region surrounding HD 37903. The coexistence of the C II region with a region of enhanced CO emission suggests that the CO in NGC 2023 may be excited by electron collisions.

Subject headings: molecules, interstellar — nebulae, individual — radio lines

I. INTRODUCTION

Radio recombination line emission from ionized carbon was recently detected from the ρ Ophiuchi dark cloud (Brown and Knapp 1974). Subsequent observations (Brown *et al.* 1974) suggested that the most reasonable interpretation of this emission is that it arises in one or several extended regions of ionized carbon surrounding early B-type stars (i.e., C II Strömgren spheres) which are embedded in the dark cloud. This suggests that the carbon line emission from the Ophiuchus cloud is not an isolated phenomenon, but rather that carbon lines should be detected from other (indeed most) suitably large, dense clouds with early-type stars embedded in them. To investigate this hypothesis, we have undertaken observations of other similar dark clouds, including the reflection nebula NGC 2023, which surrounds, and is presumably illuminated by, the B1.5 V star HD 37903. Carbon recombination line emission was detected at four frequencies at the position of the star; the characteristics of the line emission, and the physical parameters of the region, are described in §§ IV and V below.

II. THE REGION OBSERVED

Before discussing the radiofrequency observations, we will briefly describe the region containing NGC 2023. The reflection nebula NGC 2023 is in the large dark cloud L1630 (Lynds 1962) in Orion. A reproduction of part of the red *National Geographic Society-Palomar Observatory Sky Survey* print of the region is shown in figure 1. NGC 2023 is about $25'$ south of the H II region NGC 2024 (W12 or Orion B), and east of the Horsehead Nebula. L1630 extends approximately 3° east and north of the region shown in figure 1, and contains several other reflection nebulosities, including M78 (NGC 2068) and NGC 2071. The nebulosity M42 (Orion A) lies about 3° south of the Horsehead Nebula, and the whole complex is contained within Barnard's Loop. (An excellent photograph and diagram of the various emission and reflection nebulae in this region is given by Vehrenberg 1967.)

The reflection nebula NGC 2023 is about $10'$ in diameter and surrounds the star HD 37903. This star is embedded in part of L1630, suffering about 1.5 mag of absorption (Sharpless 1952). Within a few arc minutes of the star are the H α emission-line star LkH α 287, and about 10 very faint reddish stars, seen at near-infrared wavelengths (S. E. Strom and K. M. Strom 1974), which are interpreted as B- and A-type stars obscured by about 10 mag of visual absorption.

Not apparently physically connected with NGC 2023 are the H II regions NGC 2024 and IC 434. NGC 2024 is a fairly compact H II region, whose exciting star, of early B-type, is heavily obscured by the dust lane crossing the region (Grasdalen 1974). The western boundary of L1630 is very sharp, and can be seen projected against the diffuse H II region IC 434, which is excited by ζ Ori (spectral type O9.5 Ib) and σ Ori (type O9.5 V).

The whole region described above appears to be a very active area of star formation, as shown by the presence of the many emission and reflection nebulae, and by the numerous early-type emission-line and T Tauri stars (e.g., Haro and Moreno 1953; Herbig and Kuhl 1973; Strom *et al.* 1974). NGC 2023 was observed at four frequencies; two of the beamwidths used are shown in figure 1.

* Operated by Associated Universities, Inc., under contract with the National Science Foundation.

At radio frequencies, this region is also of great interest. Apart from Orion A and Orion B, both of which show strong carbon recombination line emission in their spectra—see, for example, Zuckerman and Ball (1974)—an OH maser source has been detected in NGC 2071 (Johansson *et al.* 1974). Observations of CO in this region (Tucker, Kutner, and Thaddeus 1973; Milman *et al.* 1974; Wannier 1974) show several peaks in the intensity of the CO emission, the most intense being at the position of NGC 2023. Thus the recombination line results to be described in the present work may prove very useful for understanding the distribution of the CO excitation temperature (see § V).

III. MULTIFREQUENCY RECOMBINATION LINE OBSERVATIONS

a) *The Observational Philosophy*

Considerable caution must be exercised in the interpretation of the observations of recombination lines which arise in a cold, partially ionized gas if one wishes to establish the average physical parameters (n_e = electron density in cm^{-3} ; T_e = electron temperature) in the emission region, because the expected line intensity may be a strong function of these parameters (e.g., Brown and Gómez-González 1974). In particular, the recombination line emission and absorption coefficients (or the line optical depth) may be very sensitive to small changes in the electron density or temperature through variations in the non-LTE departure coefficients b_n and their variation with frequency $d(\ln b_n)/dn$. In a sense this variation is fortunate, because it allows one to establish the values of n_e and T_e for a particular source *if one can study the variation of line intensity as a function of principal quantum number*. Hence, observations at more than one frequency are obligatory; we report below detection of the C 76 α , C 110 α , C 142 α , C 166 α , and C 167 α lines in NGC 2023, and examine their implications for the physical parameters of the region in §§ IV and V.

Unfortunately, a comparison of line observations at several frequencies is not entirely straightforward since such observations are generally made with differing telescope beamwidths. Hence, the comparison can be meaningful only if one has an *a priori* knowledge of the size of the emitting region relative to the beamwidth at each frequency. In an attempt to minimize such uncertainties, we have observed the same line (actually the adjacent C 166 α and C 167 α lines) with two telescopes whose beamwidths differ by a factor of 2; in this manner it is feasible to estimate the beam-filling factor. We have also observed two different lines (the C 142 α and C 166 α lines) with the same beamwidth.

b) *The Observations*

The observations were made with three different telescopes—the NRAO 140-foot (43 m) and 300-foot (91 m), and the Goldstone 85-foot (26 m) telescopes—in a period between 1973 November and 1974 April. The individual observations are described below. For all observations except the 6-cm (110 α) observations, one point, centered at the position of HD 37903, was observed. The position is:

$$\alpha = 05^{\text{h}}39^{\text{m}}07^{\text{s}}, \quad \delta = -02^{\circ}16'58'' \quad (1950).$$

The galactic coordinates of this point are $l = 206^{\circ}9$, $b = -16^{\circ}5$. For the C 110 α line observations the beam was centered 1' south of the above position. The observations are summarized in table 1; also given in table 1 are the observed CO line parameters at the above position as given by Milman *et al.* (1974).

c) *The C 166 α and C 167 α Observations*

Observations of these lines, whose frequencies are at ~ 1425 and 1400 MHz, respectively (and which we regard as equivalently the same line), were made in 1973 December with the NRAO 43 m telescope (C 167 α), and in 1974 April with the NRAO 91 m telescope (C 166 α). In both cases, the front end used for the observations was a cooled

TABLE 1
RECOMBINATION LINE OBSERVATIONS OF NGC 2023

Line	ν (GHz)	Ω_B	T_A (° K)	v_{LSR} (km s $^{-1}$)	Δv (km s $^{-1}$)	P (° K-kHz)
C 76 α	14.7	2:2	0.026 ± 0.009	10.4 ± 0.3	1.5 ± 0.3	4.2 ± 1.7
C 110 α	4.87	6.1	0.030 ± 0.009	10.4 ± 0.3	2.0 ± 0.3	1.4 ± 0.5
*C 142 α	2.27	22	0.014 ± 0.005	10.0 ± 0.7	2.0 ± 0.7	0.32 ± 0.16
C 167 α	1.40	21	0.045 ± 0.008	10.5 ± 0.4	2.1 ± 0.4	0.60 ± 0.15
†C 166 α	1.42	10	0.04 ± 0.02	10.5 ± 0.9	2.6	(0.70)
‡ ¹² CO	115	1:2	34	10.3	2.6	...
‡ ¹³ CO	110	1:2	11	10.0	2.1	...

* Observation taken with the NASA–Goldstone 26 m Venus telescope (DSS-13).

† Observation taken with the NRAO 91 m telescope.

‡ From Milman *et al.* (1974).

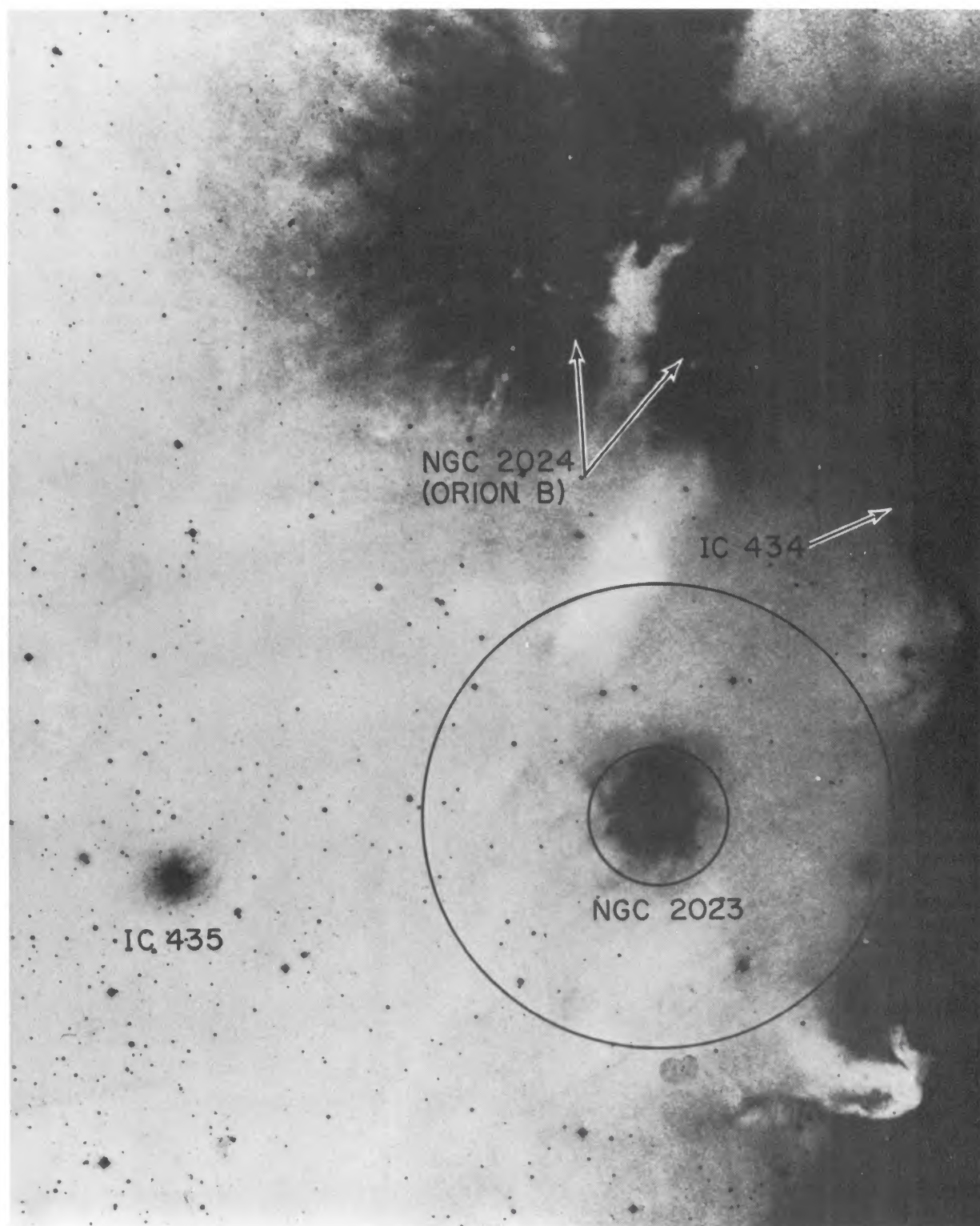


FIG. 1.—Part of the dark cloud L1630 in Orion, containing the Horsehead Nebula, IC 434, NGC 2024, NGC 2023, and IC 435. The 21' and 6' beams used to observe NGC 2023 are indicated. (Copyright by the *National Geographic Society-Palomar Observatory Sky Survey*. Reproduced by permission from The Hale Observatories.)

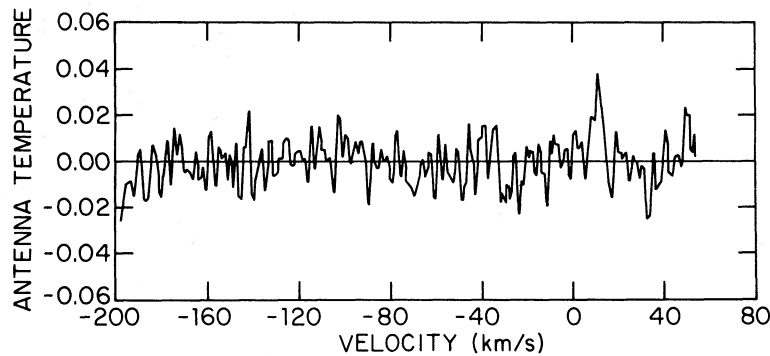


FIG. 2.—The C 167 α line profile observed at the position of NGC 2023. The velocity scale refers to the LSR velocity for the C 167 α line.

dual-channel parametric amplifier providing a system temperature near 50° K. The aperture efficiency of the 43 m telescope is ~ 57 percent and the beam efficiency ~ 75 percent; the half-power beamwidth is $\sim 21'$. The spectral analysis was performed by the NRAO 413-channel autocorrelation receiver operating in its parallel mode, to observe two independent spectra over a total bandwidth of 1.25 MHz, giving a velocity resolution of 1.3 km s^{-1} . The C 167 α line was detected well above the noise, and the observed spectrum is shown in figure 2. The observed parameters of the C 167 α line are given in table 1.

As is the case with the carbon recombination lines observed in the ρ Oph dark cloud (Brown and Knapp 1974; Brown *et al.* 1974), the line is extremely narrow, with a full width at half-maximum (Δv) of $\sim 2 \text{ km s}^{-1}$. As can be seen from table 1, the central velocity of the line is identical to that of the CO emission lines at this position (Milman *et al.* 1974), and the line width is identical to that of the (presumably unsaturated) ^{13}CO line. Thus there can be no doubt that the line illustrated in figure 2 is indeed the result of radiative transitions from atomic carbon in NGC 2023. The spectral window used (see fig. 2) was wide enough to include the recombination lines of heavier atomic species (Si, S, Mg, Fe), but no such lines are seen. (This is consistent with their cosmic abundances relative to carbon.) Neither was the C 210 β line detected, although it was also included in the observed spectral range.

The aperture efficiency of the 91 m telescope at the declination of NGC 2023 is ~ 52 percent, and the beam efficiency ~ 70 percent. The spectra were observed with the NRAO 384-channel autocorrelation receiver, observing a bandwidth of 1.25 MHz across 96 channels, giving a velocity resolution of $\sim 2.6 \text{ km s}^{-1}$. The observational parameters of the C 166 α line are also given in table 1.

d) The C 142 α Observations

The C 142 α (2273 MHz) observations were made in 1974 April with the 26 m Venus telescope of the NASA Deep Space Network (DSN) at Goldstone, California. The telescope is of Cassegrain construction, with a maser-amplifier front end. The system temperature was $18^\circ\text{--}25^\circ \text{ K}$, depending on the elevation of the source. The aperture efficiency of the telescope was ~ 50 percent, and the beam efficiency ~ 65 percent. The telescope beamwidth at 13 cm is $\sim 21'$. The observations were made using a one-bit 64-channel autocorrelation receiver, with a resolution of 8 kHz ($\sim 1.3 \text{ km s}^{-1}$) per channel. The total-power observing mode was used, with a reference position 3° east of NGC 2023. The observational parameters for this line are somewhat uncertain because of nonlinear effects in the receiver baseline.

e) The C 110 α Observations

The C 110 α observations (4874 MHz) were made in 1973 November with the NRAO 43 m telescope and a cooled parametric amplifier which gave a system temperature of $\sim 60^\circ \text{ K}$; the telescope beamwidth was $\sim 6'$ and the beam efficiency ~ 65 percent. The Mark II 413-channel autocorrelation receiver was operated in parallel mode to observe the line with two different bandwidths; one bandwidth was 2.5 MHz, giving a velocity resolution of 0.8 km s^{-1} , while the other was 10 MHz, giving a resolution of 3.2 km s^{-1} . In addition to the detection of the C 110 α line, the properties of which are given in table 1, the second bandwidth was chosen to be wide enough to include the H 110 α and He 110 α lines; no hydrogen or helium recombination lines were detected.

f) The C 76 α Observations

We have also detected the C 76 α line in NGC 2023; the observational parameters for this line are summarized in table 1. The observations were made in 1973 November with the NRAO 43 m telescope, the 2-cm cooled dual-channel parametric amplifier, and the 413-channel autocorrelation receiver. The system temperature was $110^\circ\text{--}120^\circ \text{ K}$, becoming somewhat higher in cloudy weather. The beamwidth was $2.2'$, and the beam efficiency, ~ 45

percent; all of these parameters deteriorated somewhat at high zenith angles. The observations were made with the autocorrelation receiver in its parallel mode, with one bank of channels centered on the C 76 α line and the other on the H 76 α line. The bandwidth used was 10 MHz, giving a velocity resolution of $\sim 1.0 \text{ km s}^{-1}$. No hydrogen or helium recombination line emission was detected down to a level of $\sim 0.02^\circ \text{ K}$.

IV. PHYSICAL PARAMETERS IN THE C II LINE-EMITTING REGION

The observations described above fall into three general categories which lead in turn to somewhat different avenues of approach to an analysis of the physical conditions in the C II line-emitting region: (1) observations of lines of different principal quantum number with the same telescope beamwidth; (2) observations of lines of the same principal quantum number with different telescope beamwidths; (3) observations at high angular resolution. Below we consider separately the kind of perspective on the physical properties of the region provided by these different types of observation.

a) The C 167 α and C 142 α Recombination Lines

The C 167 α observations taken with the NRAO 43 m telescope have an angular resolution which is essentially identical to the C 142 α observations obtained with the NASA-DSN 26 m Venus telescope; hence the beam-filling factor for the C II source is the same in the two cases, and a comparison of the results is straightforward. Because of the different values for the beam efficiencies of the telescopes used, we compare values of the "brightness temperature," given by T_A/η_B (where T_A is the observed antenna temperature and η_B is the telescope beam efficiency; this involves the assumption that the source is extended).

The power emitted in a line of principal quantum number n is

$$P_n \simeq T_L \Delta\nu = 1.14 \times 10^4 \Lambda_n f_n b_n n^{-1} [1 - (T_0/T_e)\beta_n] T_e^{-3/2} n_e^2 l \exp\left(\frac{1.579 \times 10^5}{n^2 T_e}\right), \quad (1)$$

where Λ_n is the beam filling factor at the frequency corresponding to the line of principal quantum number n :

$$\Lambda_n \approx \Omega_S/\Omega_B, \quad (2)$$

where Ω_S and Ω_B are the solid angles subtended by the source and beam, respectively (if $\Omega_S > \Omega_B$, then $\Lambda_n \equiv 1$). The rest of the symbols in equation (1) have their usual meanings (cf. Gordon 1973). If we now consider the ratio of the power emitted in the C 142 α line ($\equiv n\alpha$) to that emitted in the C 167 α line ($\equiv m\alpha$),

$$\frac{P_n}{P_m} = \frac{b_n f_n n}{b_m f_m m} \left[\frac{1 - (T_0/T_e)\beta_n}{1 - (T_0/T_e)\beta_m} \right] \exp\left[\frac{1.579 \times 10^5}{T_e} \left(\frac{1}{n^2} - \frac{1}{m^2} \right) \right] \quad (3)$$

where we have made use of the fact that $\Lambda_n = \Lambda_m$. Since the only background stimulation arises from the 2.7° K microwave background, we employ the simplifications described by Brown *et al.* (1974) to obtain

$$T_e = 1.579 \times 10^5 \left(\frac{1}{n^2} - \frac{1}{m^2} \right) \left\{ \ln \frac{P_n n b_m f_m}{P_m m b_n f_n} \left[1 + \frac{kT_0}{h} \left(\frac{S_m}{\nu_m} - \frac{S_n}{\nu_n} \right) \right] \right\}^{-1}. \quad (4)$$

Using this equation, we can solve for values of n_e and T_e in the C II line-emitting region consistent with the observations. While such a solution is formally straightforward, one needs to know the non-LTE departure coefficients, b_n , and their slopes $S_n (=d \log b_n/dn)$ as a function of T_e and n_e in order to carry out this calculation. Adopting Dupree's (1972) results, we have solved equation (4) for $T_e = 10^\circ \text{ K}$ and 20° K for a range of possible values of the electron density; these solutions are shown graphically in figure 3. As in Brown *et al.* (1974), at each value of the electron temperature, the right side of equation (4) has been evaluated as a function of n_e , and these solutions produce the parabolic curves shown in figure 3; the horizontal line in each of the diagrams is the assumed temperature, i.e., the left side of equation (4). A solution exists only at those values of n_e at which the two curves cross. There are two such solutions for each value of T_e : if $T_e = 20^\circ \text{ K}$, $n_e = 0.2 \text{ cm}^{-3}$ or 0.08 cm^{-3} ; if $T_e = 10^\circ \text{ K}$, $n_e = 0.5 \text{ cm}^{-3}$ or 0.03 cm^{-3} . Much higher values of the temperature (e.g., $T_e \simeq 100^\circ \text{ K}$) give no viable solutions.

b) The C 166 α Recombination Line

Before attempting any further analysis of the C 167 α and C 142 α data taken with beamwidths of 21', we need to estimate the fraction of the beam solid angle which is filled by the line-emitting region. To do this, we have also observed the C 166 α line with the NRAO 91 m telescope, which provides an angular resolution of 10' at this frequency, or roughly half that of the 43 m telescope. The ratio of the power in the C 166 α line observed with 10' resolution to that observed with 21' resolution is (see eq. [1])

$$\frac{P(10')}{P(21')} = \left[\frac{\Omega_S(10')}{\Omega_S(21')} \right] \left[\frac{\Omega_B(21')}{\Omega_B(10')} \right]. \quad (5)$$

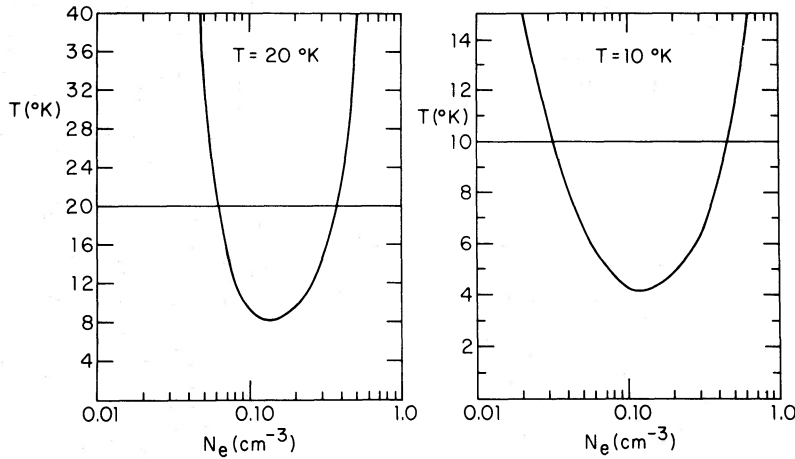


FIG. 3.—Graphical display of the solutions to eq. (4) consistent with the recombination line observations of NGC 2023. A solution is found only at the crossing points of the two curves for each temperature shown.

There are two limiting cases: (1) if the size of the line-emitting region is as large as 21' or larger, then $\Omega_s(10') \equiv \Omega_B(10')$ and $\Omega_s(21') \equiv \Omega_B(21')$, so that $P(10')/P(21') = 1$; (2) alternatively, if the size of the line emitting region is 10' or smaller, then $\Omega_s(10') = \Omega_s(10')$ and $P(10')/P(21') = (21/10)^2 = 4.4$.

Comparing these limits to the observations (table 1), we see that the observed ratio is

$$\left[\frac{P(10')}{P(21')} \right]_{\text{obs}} = 1.2 \pm 0.5. \tag{6}$$

Equation (6) shows that the line-emitting region at 21 cm is certainly as large as 10' and perhaps as large or larger than 21'.

We may now assume $\Lambda_{167} \simeq 1$, and use the observed power in the C 167 α line together with equation (1) to calculate the emission measure for each of the possible values of T_e and n_e derived in § IV a above. The results are given in table 2. Also given in this table is the line-of-sight dimension of the line-emitting region in both parsecs and minutes of arc (assuming a distance of 450 pc to NGC 2023), which is directly obtainable from the derived values of n_e and the emission measure, $n_e^2 l$.

At this point, we note that if the line-emitting region surrounds and is excited by HD 37903, the illuminating star of NGC 2023—and we present arguments below to suggest that this is in fact the case—then the line-of-sight dimension is the characteristic dimension of the emission region. With this in mind, table 2 shows that both possible values of n_e at $T_e = 10^\circ \text{ K}$ are incompatible with the observations ($n_e = 0.5 \text{ cm}^{-3}$, because the emission region is much smaller than the 10' beam; and $n_e = 0.03 \text{ cm}^{-3}$, because the required linear dimension is prohibitively large); similarly, the $T_e = 20^\circ \text{ K}$, $n_e = 0.08 \text{ cm}^{-3}$ solution is probably unacceptable because it requires an emission path length far larger than could be ionized by HD 37903.

We conclude that the mean parameters averaged over a 21' beam characteristic of the C II region surrounding HD 37903 which are consistent with the recombination line observations are $T_e \simeq 20^\circ \text{ K}$ and $n_e \simeq 0.2 \text{ cm}^{-3}$.

c) The C 110 α and C 76 α Recombination Lines

These observations, which sample the characteristics of the line-emission region with high angular resolution, 6' (C 110 α) and 2' (C 76 α), respectively, were undertaken to demonstrate the association of HD 37903, the illuminating star of NGC 2023, with the recombination line region.

TABLE 2
DERIVED PARAMETERS OF THE NGC 2023 C II REGION

Parameter	Emission measure $n_e^2 l$ ($\text{cm}^{-6} \text{ pc}$)	l (pc)	Size ϕ (min)	$\frac{\langle n_e^2(6') \rangle}{\langle n_e^2(21') \rangle}$	$\frac{\langle n_e^2(2') \rangle}{\langle n_e^2(21') \rangle}$
$T_e = 20^\circ \text{ K}$:					
$n_e = 0.2 \text{ cm}^{-3}$	0.061	1.5	11	5.5	31
$n_e = 0.08 \text{ cm}^{-3}$	0.074	12	91	(6.1)	(23)
$T_e = 10^\circ \text{ K}$:					
$n_e = 0.5 \text{ cm}^{-3}$	0.013	0.052	0.4	(7.0)	(52)
$n_e = 0.03 \text{ cm}^{-3}$	0.038	42	320	(5.4)	(31)

From § IVa, we have an estimate of the mean n_e and T_e in the C II region, and from § IVb we know that the beam-filling factor for the 21' observations is $\simeq 1$, so that certainly $\Lambda_{110} \simeq \Lambda_{76} \simeq 1$ for the high resolution observations discussed here, if the C II region is of uniform surface brightness. In this case we may use equation (3) to calculate the expected ratio of the power in the C 110 α line or the C 76 α line to the power in the C 167 α line as

$$\frac{P_{110}}{P_{167}} = \frac{b_{110}}{b_{167}} \exp \left[\frac{1.579 \times 10^5}{T_e} \left(\frac{1}{110^2} - \frac{1}{167^2} \right) \right] \approx 0.42, \quad (7)$$

(where we have used $|(T_0/T_e)\beta| \ll 1$). This result is very much smaller than the observed ratio $P_{110}/P_{167} \approx 2.3$. Similarly, if we compare the expected P_{76}/P_{167} ratio to that observed, we find that the former exceeds the latter by a factor of ~ 31 . The conclusion which follows from this is, simply stated, that the surface brightness of the carbon recombination line emission increases as the beamwidth (centered on the star) decreases. This conclusion provides compelling support for the assertion that the C II region which we are observing surrounds and is excited by photons $\lambda\lambda 912$ – 1100 provided by HD 37903, the illuminating star of NGC 2023 itself.

Now, from equation (1), we see that the power in the line at a particular value of n will increase if either n_e^2 is larger near the star than the mean n_e^2 determined from the 21' observations, or if T_e is smaller near the star than in the surrounding gas. The latter possibility is unlikely both because one expects the temperature to *increase* as one approaches the star (if indeed there is any change at all), and because the electron temperature required to be consistent with the observations is $T_e \lesssim 3^\circ$ K, and this value is in marked conflict with the CO results for this region (Tucker *et al.* 1973; Milman *et al.* 1974). Hence we conclude that the mean electron density on a scale of 2' or 6' centered on NGC 2023 is greater than the mean electron density determined from the 21' observations. In this case, we can write the ratio of the power in the C $n\alpha$ line as observed with a beam solid angle of Ω_n to the power in the C $m\alpha$ line observed with a beam solid angle Ω_m as

$$\frac{P_n}{P_m} \simeq \frac{b_n \langle n_e^2(\Omega_n) \rangle}{b_m \langle n_e^2(\Omega_m) \rangle} \exp \left[\frac{1.579 \times 10^5}{T_e} \left(\frac{1}{n^2} - \frac{1}{m^2} \right) \right], \quad (8)$$

where $\langle n_e^2(\Omega_n) \rangle$ is the mean value of the square of the electron density averaged over a telescope beam of solid angle Ω_n .

The C 167 α and C 142 α lines provide a reliable estimate of $\langle n_e^2(21') \rangle$ as determined in § IVa, so that we may use equation (8) together with the observed power in the C 167 α line and the power in the C 110 α and C 76 α lines to obtain an estimate of the mean electron density within 6' and 2', respectively, of NGC 2023; the results relative to $\langle n_e^2(21') \rangle$ are given in table 2. While all the columns of this table are filled in, recall from the arguments of § IVb that only the top line—the $T_e = 20^\circ$ K, $n_e = 0.2 \text{ cm}^{-3}$ model—is entirely consistent with what we know about the source. We conclude, therefore, that the mean square electron density increases toward the star with decreasing beamwidth. The form of the density increase with angular size ϕ can be fitted equally well to a power law or an exponential, viz.,

$$\langle n_e^2(\phi) \rangle = \langle n_e^2(21') \rangle \left(\frac{\phi}{\phi_{21}} \right)^{-3/2}, \quad (9)$$

with $\phi_{21} = 21'$, or

$$\langle n_e^2(\phi) \rangle^{1/2} = \langle n_e^2(0) \rangle^{-1/2} \exp(-\phi/\phi_0), \quad (10)$$

with $\phi_0 = 10'$ and $\langle n_e^2(0) \rangle^{1/2} = 1.5 \text{ cm}^{-3}$.

Here $\phi = r/d$, where r = radial distance from the star and d = distance to NGC 2023 (assumed to be 450 pc). In either case, when we infer an increase in $\langle n_e^2(\phi) \rangle$ with decreasing ϕ , we may be observing either (a) a uniform gas in which the fractional C⁺/C ratio increases with decreasing ϕ , or (b), an increase in total density in which the C⁺/C ratio is constant; with the present observations we cannot distinguish between these possibilities.

V. DISCUSSION: THE NGC 2023 C II REGION

a) Summary of the Observational Properties

A brief summary of the observational and derived properties of the carbon recombination line region NGC 2023 is as follows: (1) the line emission arises in a region comparable with 21' in angular size; (2) the lines are narrow— $\Delta v \sim 2 \text{ km s}^{-1}$; (3) the characteristic thermal parameters of the ionized region averaged over a 21' beam are $T_e \sim 20^\circ$ K, $n_e \sim 0.2 \text{ cm}^{-3}$; (4) the mean electron density increases as one observes with smaller telescope beams closer to the star. The simplest, and indeed the most reasonable, interpretation of these results is that the recombination line emission arises in the dense, cold gas surrounding NGC 2023; the carbon ionization is provided by stellar photons $\lambda\lambda 912$ – 1100 emitted by HD 37903 (the illuminating star of NGC 2023) which escape the highly compact H II region immediately surrounding the star and are absorbed in the more extended surrounding medium. A look at the energy balance involved reinforces this conclusion.

b) *The Energetics of the C II Region NGC 2023*

HD 37903 is a B1.5 V star, which, using the line-blanketed model atmospheres of Van Citters and Morton (1970) and stellar radii estimated by Panagia (1973), should emit $\sim 2.2 \times 10^{46}$ photons per second capable of ionizing carbon. From the recombination line data we can estimate the number of carbon-ionizing photons needed to explain the observations by

$$L_c = \int n_e n(C^+) \alpha(C) dV, \quad (11)$$

where $\alpha(C)$ is the recombination coefficient for carbon in $\text{cm}^3 \text{s}^{-1}$. If we assume, first, that the star is surrounded by a uniform-density gas at $T_e = 20^\circ \text{K}$ and $n_e = n(C^+) = 0.2 \text{ cm}^{-3}$, as indicated by the averaged parameters over a $21'$ beam (§ IVa, b), then we require

$$L_c \simeq 6 \times 10^{44} \text{ photons s}^{-1} \text{ (uniform density)}.$$

Since the number of carbon-ionizing photons far exceeds this requirement, HD 37903 can easily provide the necessary ionization if the density is uniform.

In § IV c, we concluded from the high-resolution observations that the electron density should be larger near the star than in the more extended region observed with the $21'$ beam. If we assume that the density distribution is as given by the power law (eq. [9]) and evaluate equation (11), we find that the required number of carbon-ionizing photons exceeds 10^{50} s^{-1} , a number which is several orders of magnitude more than HD 37903 (or the 10 possible B-A stars embedded in this same region) can provide. Hence, we conclude that this density distribution is untenable. This conclusion is supported by a comparison of the antenna temperature of the C 167 α line ($21'$ beam) and the C 166 α line ($10'$ beam): the power-law distribution (eq. 9) is so centrally concentrated that we would expect the ratio of the antenna temperatures to be about 4, whereas in fact this ratio has a value close to 1 (cf. § IVb).

Let us instead consider the exponential density distribution (eq. 10), which is also consistent with the high and low angular resolution observations. Substituting this expression in equation (11), we find that the number of carbon-ionizing photons necessary to explain the observations is

$$L_c \simeq \pi \langle n_e^2(0) \rangle \alpha(C) \phi_0 d^3 \simeq 1.6 \times 10^{46} \text{ photons s}^{-1}, \quad (12)$$

which is very close to the number of such photons emitted by HD 37903. Such reassuring agreement provides additional support for the model in which the C II region is an extended Strömgen sphere-like region of ionized carbon (also ionized S, Si, Fe, Mg, etc.) having a scale size $\geq 10'$, and surrounding both a very compact H II region (with angular scale size of a few arc sec) and its exciting B-type star. The radius of the C II region is determined by absorption by dust grains, and is $\sim 325/n(\text{H})$ pc (Brown *et al.* 1974), or about 1 pc at the average density of L1630, consistent with the observations.

c) *The H II Region Surrounding HD 37903*

Let us consider briefly the properties of the compact H II region which must surround HD 37903. Again using the Van Citters and Morton (1970) line-blanketed model atmospheres together with Panagia's (1973) estimate of the radius appropriate to a B1.5 V star, we find that HD 37903 emits 1.4×10^{45} Lyman continuum photons per second. Hence the angular size $\phi_{\text{H II}}$ of the H II region surrounding the star is

$$\phi_{\text{H II}} = 14'' \left[\frac{n(\text{cm}^{-3})}{1000} \right]^{2/3}. \quad (13)$$

From equation (10) and the estimate (§ IVb) of the mean density of ionized carbon, $\langle n_e \rangle \simeq \langle n(C^+) \rangle \simeq 0.2 \text{ cm}^{-3}$, we surmise that $500 \leq n \leq 4000 \text{ cm}^{-3}$, so that

$$25'' \leq \phi_{\text{H II}} \leq 5''. \quad (14)$$

The thermal continuum radiofrequency flux emitted from this H II region is $\sim 25\text{--}40$ mJy at 5000 MHz. Observations at 2695 and 8085 MHz with the NRAO three-element interferometer reveal the presence of at least two sources of strength approximately 25 mJy, but both are displaced about $3'$ from NGC 2023; the (3σ) upper limit to the continuum flux coincident with HD 37903 is about 15 mJy (Brown and Broderick 1974). However, single-dish observations show the presence of low-level continuum radiation at the position of NGC 2023. Kuiper (1974) has detected a source of strength ~ 50 mJy at 2.37 GHz; the existence of this source is also suggested on the 2.7 GHz map of Caswell and Goss (1974).

These observations thus suggest that the H II region immediately surrounding HD 37903 is of the order of 0.5 in diameter, so that the mean density is quite low, of the order of $500\text{--}1000 \text{ cm}^{-3}$. This H II region is too small to give rise to detectable recombination line emission from H or He, as is borne out by the observational results described above.

d) Comparison with CO Observations near NGC 2023

We referred earlier to the association of NGC 2023 with a local maximum in the CO brightness temperature; at this position $T_B(^{12}\text{CO}) = 34^\circ \text{K}$ (Milman *et al.* 1974). Since the surface brightness of the recombination line emission, and, by inference, the local value of the density, also peaks at this position, it seems reasonable to conclude that the CO and ionized carbon are colocated; the agreement between the velocities and velocity widths of the CO and recombination lines reinforces this conclusion. The illuminating star or stars of NGC 2023 are then the ultimate source of both the carbon ionization and the high CO brightness temperature at this position.

In dust clouds, the main isotopic species, ^{12}CO , is almost always observed to be heavily saturated, and the NGC 2023 region is no exception; thus spatial variations in the observed brightness temperature of the line directly reflect spatial variations in the excitation temperature of the molecule. In the NGC 2023 region, the peak ^{12}CO brightness temperature has a maximum value close to the position of HD 37903 (corresponding to an excitation temperature of 38°K), and falls off around the star, with the approximate angular size of the region of enhanced brightness temperature being about $25'$, or roughly the size of the recombination line region. The co-existence of the C II region and the region of enhanced ^{12}CO brightness temperature suggests that the CO near HD 37903 may be excited above the typical dust cloud temperature of $\sim 10^\circ \text{K}$ by collisions with free electrons in the C II region. Furthermore, the mean CO excitation temperature averaged over this region is $\sim 25^\circ \text{K}$, close to the value of the electron density derived above.

Observations of the ^{13}CO line in this region, on the other hand, show the region of enhanced brightness temperature to be confined to a much smaller region, $\sim 6'$, near the star. Since $\tau(^{13}\text{CO}) \ll 1$, variations in the spatial distribution of the ^{13}CO line are directly related to variations in the column density, and we conclude that the ambient density in the gas surrounding HD 37903 increases towards the star, as is also indicated by the recombination line data discussed above.

Both the C⁺ observations of the present paper and the CO observations (Milman *et al.* 1974) show no detectable change in the line width close to HD 37903. This is quite consistent with the low gas temperature inferred from the present observations, since the presumed increase of the sound speed of the gas in the hotter region near HD 37903 is only a few tenths of a km s^{-1} . Thus HD 37903 (and any other early-type star in the vicinity) is imparting essentially no expansion or turbulent motions to the gas around it, a situation quite different from that in H II regions surrounding O-type stars (see, e.g., Mathews and O'Dell 1969).

e) Comparison with the ρ Ophiuchi Dark Cloud

Finally, a brief comparison between the carbon recombination line emission in NGC 2023 and that seen in the ρ Oph dark cloud (Brown and Knapp 1974; Brown *et al.* 1974) seems warranted. The similarities are many: the carbon recombination line widths are $\sim 2 \text{ km s}^{-1}$; no hydrogen line is seen; the emission occurs near B-type stars embedded in the cloud; the electron temperature is $\sim 20^\circ \text{K}$ in both cases; CO emission is detectable over a wide area of the cloud adjacent to and including the source of the recombination line emission. The most striking feature of the ρ Oph dark cloud is the existence of numerous point sources detected in the near-infrared which are inferred by Grasdalen, Strom, and Strom (1973) to be highly obscured B-type stars; the cloud has also been detected in the far-infrared, 350μ , at some of these positions (Simon *et al.* 1973). Interestingly, Strom and Strom (1974) also report near-infrared detections of several late B and early A-type stars with ~ 10 mag of visual absorption within a few arc min of HD 37903. Apparently, the two carbon recombination line regions are quite similar; if this is so, an observation of the region near NGC 2023 at 350μ should be profitable.

Not all conditions are the same in the ρ Oph dark cloud and the NGC 2023 region; the most conspicuous difference noticeable from the recombination line observations is that the electron density (and presumably the total density) is higher by about a factor of 5 in the ρ Oph cloud than in the cold gas surrounding HD 37903, while the temperature is probably lower.

The present study reinforces the interpretation (Brown *et al.* 1974) of the carbon recombination line emission in the ρ Oph cloud—viz., that it arises in one or several C II regions surrounding B-type stars embedded in a dense obscuring cloud—because, in the case of NGC 2023, there is no ambiguity as to the star (and its spectral type) which serves as the source of ionization. We conclude from these observations that the phenomena we are observing, namely carbon recombination line emission from extended Strömberg spheres of cold ionized carbon, silicon, sulfur, iron, magnesium, etc., surrounding B-type stars, should be so common and widespread that carbon recombination line emission should be detectable from many nearby, obscured, B-type stars.

We would like to express many thanks to Dr. R. H. Gammon and Dr. B. Balick for providing the 6-cm observations used in this paper, and to Mr. A. S. Milman for drawing our attention to this interesting region. We are very grateful to the National Radio Astronomy Observatory and the Venus-Goldstone station of the NASA-JPL Deep Space Network for granting the observing time used in this project, and to the staff for their part in the observations. We particularly thank Mr. G. A. Morris for much help with the Goldstone observations. During some of the observations, G. R. K. was partly supported by the National Science Foundation under grant GP-27503 to the University of Maryland. Research at the Owens Valley Radio Observatory is supported by the Office of Naval Research under contract N00014-67-A-0094-0019, and by the NSF under grant GP-30400-XI. This paper presents

the results of one phase of research carried out at the Jet Propulsion Laboratory, California Institute of Technology, under contract NAS 7-100, sponsored by the National Aeronautics and Space Administration. T. B. H. K. is an NRC Resident Research Associate at the Jet Propulsion Laboratory.

REFERENCES

- Brown, R. L., and Broderick, J. J. 1974, in preparation.
 Brown, R. L., and Gómez-González, J. 1974, *Ap. J.* (submitted).
 Brown, R. L., and Knapp, G. R. 1974, *Ap. J.*, **189**, 253.
 Brown, R. L., Gammon, R. H., Knapp, G. R., and Balick, B. 1974, *Ap. J.*, **192**, 607.
 Caswell, J. L., and Goss, W. M. 1974, *Astr. and Ap.*, **32**, 209.
 Dupree, A. K. 1972, *Ap. J.*, **173**, 293.
 Gordon, M. A. 1973, *Ap. J.*, **184**, 77.
 Grasdalen, G. 1974, *Ap. J.*, **193**, 373.
 Grasdalen, G., Strom, K. M., and Strom, S. E. 1973, *Ap. J. (Letters)*, **184**, L53.
 Haro, G., and Moreno, A. 1953, *Bol. Obs. Tonantzintla y Tacubaya*, **7**, 11.
 Herbig, G. H., and Kuhl, L. V. 1963, *Ap. J.*, **137**, 398.
 Johansson, L. E. B., Höglund, B., Winnberg, A., Nguyen Quang Rieu, and Goss, W. M. 1974, *Ap. J.*, **189**, 455.
 Kuiper, T. B. H. 1974, in preparation.
 Lynds, B. T. 1952, *Ap. J. Suppl.*, **7**, 1.
 Mathews, W. G., and O'Dell, C. R. 1969, *Ann. Rev. Astr. and Ap.*, **7**, 67.
 Milman, A. S., Knapp, G. R., Kerr, F. J., Knapp, S. L., and Wilson, W. J. 1974, *Ap. J.* (submitted).
 Panagia, N. 1973, *A.J.*, **78**, 929.
 Sharpless, S. 1952, *Ap. J.*, **116**, 251.
 Simon, M., Righini, G., Joyce, R. R., and Gezari, D. Y. 1973, *Ap. J. (Letters)*, **186**, L127.
 Strom, K. M., Strom, S. E., Carrasco, L., and Vrba, F. J. 1974 (preprint).
 Strom, S. E., and Strom, K. M. 1974, private communication.
 Tucker, K. D., Kutner, M. C., and Thaddeus, P. 1973, *Ap. J. (Letters)*, **186**, L13.
 Van Citters, G. W., and Morton, D. C. 1970, *Ap. J.*, **161**, 695.
 Vehrenberg, H. 1967, *An Atlas of Deep Sky Splendors* (Düsseldorf: Treugesall).
 Wannier, P. G. 1974, private communication.
 Zuckerman, B. M., and Ball, J. A. 1974, *Ap. J.*, **190**, 35.

ROBERT L. BROWN: National Radio Astronomy Observatory, Edgemont Road, Charlottesville, VA 22901

GILLIAN R. KNAPP: Owens Valley Radio Observatory, California Institute of Technology, Pasadena, CA 91125

THOMAS B. H. KUIPER: 183B-365, Jet Propulsion Laboratory, California Institute of Technology, Pasadena, CA 91101